A novel plasma test rig for auto-ignition studies of turbulent non-premixed flows

F. Eitel[1], J. Pareja[1,2], D. Geyer[3], A. Dreizler[*, 1,2]

[1]Reaktive Strömungen und Messtechnik, Technische Universität Darmstadt, Jovanka-Bontschits-Straße 2, 64287 Darmstadt, Germany

[2]Darmstadt Graduate School of Excellence Energy Science and Engineering, Technische Universität Darmstadt, Jovanka-Bontschits-Straße 2, 64287 Darmstadt, Germany

[3]Thermodynamik und Alternative Antriebe, Hochschule Darmstadt, 64285 Darmstadt, Germany

Abstract

In this paper, the development and characterization of a novel test rig for auto-ignition (AI) studies of a fuel jet propagating into a hot turbulent co-flow is reported. The test rig, based on microwave plasma-heating, is capable of achieving co-flow temperatures up to 1300 K and velocities up to 40 ms^{-1}. Lift-off height (LOH) measurements of CH_4, C_2H_4, and CH_4/H_2 jets, propagating into a turbulent air co-flow, were carried out using chemiluminescence imaging. Effects of the temperature and Reynolds number (Re) of co-flow and jet were also studied. Results showed that the flame stabilization mechanism is supported substantially by AI rather than pure flame propagation. While the co-flow temperature dominates the AI process, the Re and temperature of the jet have a small impact on the LOH.

Introduction

Auto-ignition (AI) plays an important role in a variety of combustion applications. AI is necessary to initiate the combustion in diesel engines, homogeneous charge compression ignition engines, and flameless combustors [1]. On the other hand, lean premixed prevaporized gas turbines [2] are an example of a technology in which AI needs to be avoided. In these applications fuel and air flows are usually turbulent; hence it is essential to understand the AI of turbulent flowing mixtures.

In practice, fuel is injected into a hot gaseous turbulent oxidizer. During the turbulent mixing, chemical processes such as fuel decomposition, low-temperature hydrocarbon oxidation reactions, or build-up of radicals proceed simultaneously and partly at similar time-scales to those of turbulence. Due to local variation of temperature, fuel-air-ratios, shear, etc., AI is influenced by specific physical and chemical properties of the flow as well as by turbulence-chemistry interactions.

Studies on AI of flowing mixtures have been addressed substantially through simulations [2-4]. However, experiments of a fuel jet propagating into a hot co-flow have been carried out to mimic AI conditions as those during practical processes. H_2 [5], hydrocarbons [6-7] and hydrocarbon/H_2-mixtures [8] have been used as fuels. The co-flow can be either electrically-heated air [9] or air mixed with hot combustion products, usually from lean H_2/air combustion [10]. Despite these approaches, there is still a gap of available experimental data at high co-flow temperatures in combination with high co-flow velocities and high turbulence intensities [2].

To fill this gap a new test rig for AI studies of a fuel jet propagating into a hot turbulent air co-flow has been developed. This paper is intended to provide a detailed description of the test rig, which was designed to meet requirements of well-controlled boundary conditions at much higher temperatures (up to 1300 K), velocities and Reynolds numbers (Re) of the co-flow than those accessible in previous experiments. We provide a discussion of the most important inflow boundary conditions of selected operational conditions. Although the test rig was developed with a particular emphasis on the application of a variety of laser diagnostic techniques, studies of lift-off heights were carried out as a starting point for more comprehensive investigations of the AI of turbulent non-premixed flows.

Novel auto-ignition test rig using a plasma heater

A novel AI test rig was developed using a new co-flow heating device, which is able to achieve bulk exit velocities of up to 30 ms^{-1} with adjustable turbulence levels, temperatures above 1300 K, and a top-hat temperature distribution in radial direction within the region of interest. The design allows having short heat-up times and long term temperature stability of the co-flow. A control unit reduces any temperature variations within the duration of the experiments as well as from day-to-day. The test rig, schematically represented in Fig. 1, consists of three main sections and a control unit:

(1) Microwave plasma heater (MWPH)

The MWPH used to heat up the air co-flow can be classified as a semi-metallic plasma torch [11, 12]. Microwaves are provided by a magnetron (Mügge GmbH, CWM-75L) working at 915 MHz and a maximum power of 75 kW. A waveguide guides the microwaves (marked as "G" in Fig. 1) onto a reflection plate ("F" in Fig. 1). At a distance of $\lambda_{MW}/4$ (~0.328 m) in front of the reflection plate, a standing wave forms a maximum power that energizes the air plasma ("C" in Fig. 1). The position of the electrical field distribution can be changed by a three stub tuner ("E" in Fig. 1) to optimize the power conversion. An open ended fused silica tube ("B" in Fig. 1) with an inner diameter of 115 mm and a length of 500 mm encloses the plasma. This tube is shielded by a heat resistant stainless steel tube ("M" in Fig. 1, UNS S31000) to contain electromagnetic radiation emission from the plasma.

* Corresponding author: dreizler@csi.tu-darmstadt.de

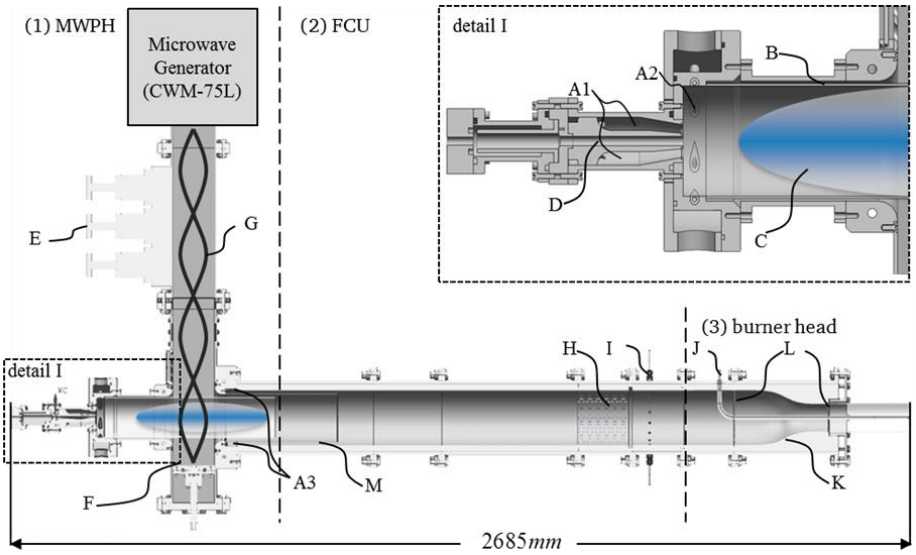

Fig. 1. Schematic cross-section of the auto-ignition test-rig.

The plasma is ignited at low microwave power (15 kW) by a copper lance that is laterally moved along the centerline (marked as "D" in Fig. 1) of the fused silica tube into the area of the power maximum for a short period of time (~0.5 s). Depending on the operation condition, the fully developed plasma absorbs 92 to 98 % of the microwave energy.

The co-flow air is supplied into the AI rig at three different inlets. All mass flows are controlled by digital mass flow controllers (MFCs, IN-Flow/EL-Flow, Bronkhorst). The first inlet (see Fig. 1, "A1" and "A2" in detail I) is used to feed air to the plasma device by a swirl generating nozzle. Air is injected through the nozzle in tangential ($\dot{m}_{tang}$) and axial ($\dot{m}_{axial}$) directions ("A2" and "A1", respectively). For stable plasma operation, the ratio $\dot{m}_{tang}/\dot{m}_{axial}$ needs to be adapted to the specific operational conditions and it is varied in the range from 3.1 to 5.5. The second air inlet ($\dot{m}_{cool} = 0.1 * \dot{m}_{axial}$) is tangentially injected directly after the MWPH ("A3" in Fig. 1) through four injection holes arranged circumferentially to cool the electromagnetic shielding tube and reduce the extremely high temperature of the air downstream of the plasma. Finally, the third air inlet ("I" in Fig. 1) can be used as seeding carrier gas for particle-based velocimetry techniques such as PIV.

(2) Flow conditioning unit (FCU)

The FCU is composed of a tube-in-tube system with an outer tube of stainless steel (UNS S30815, 200 mm inner dia.) surrounding a high temperature ceramic tube (W.E.C. Pritzkow Spezialkeramik, 80%Al_2O_3/20% SiO_2, 160 mm inner dia.). After the injection of cooling air from "A3" into the hot air issuing from the MWPH, the temperature profile is homogenized using a ceramic static mixer ("H" in Fig. 1, W.E.C. Pritzkow Spezialkeramik, material MvM17-1111P). Upstream of the static mixer additional pipe segments can be added to extend the distance between the plasma torch and the static mixer. The current distance is 895 mm and the test rig has been operated for more than 200 h with no observable degradation of the ceramic mixer. Downstream of the static mixer seeding particles can be added using the air inlet "I" ($\dot{m}_{seeding}$). The carrier gas is injected in jet-in-cross-flow configuration through 16 uniformly-distributed nozzles (3 mm inner dia.) to ensure a homogeneous temperature distribution.

(3) Burner head

Following the seeding section the burner head is attached to the FCU. The flow is accelerated by a contoured nozzle with a contraction area ratio of 4. Up- and downstream of the contraction, two turbulence enhancing perforated plates ("L" in Fig. 1, UNS S30815) with a whole diameter of 8 mm and a blockage ratio of 35 % are employed to control the integral length scale. The modular design allows a variation of turbulence levels and length scales by inserting different perforated plates. Into the contraction nozzle a jet tube ("J" in Fig. 1) guides the fuel to the exit of the burner head. This fuel lance has an inner diameter $D_{l,jet}$ = 6 mm. Heat transfer from the co-flow into the fuel flow inside the inner tube is minimized by a by ceramic shielding (W.E.C. Pritzkow Spezialkeramik, sheet ceramic). The fuel mass flow is controlled by a MFC (EL-Flow, Bronkhorst). The burner exit is attached downstream of the contraction nozzle as shown in Fig. 2. It consists of a tube of fused silica, which guides the co-flow and is aligned concentrically to the fuel lance. At the exit, the fused silica tube and the fuel lance are staggered by 5 mm to allow for full optical access directly at start of fuel injection. At the burner head exit (Fig. 2), bulk velocities of the hot co-flow, $u_{co-flow}$, are calculated by:

$$u_{co-flow} = \frac{\dot{m}_{co-flow}}{\rho(T_{co-flow-ctrl}) * \frac{\pi}{4} * (D_{O,co-flow}{}^2 - D_{I,co-flow}{}^2)} \quad (1)$$

where $\dot{m}_{co-flow} = \dot{m}_{tang} + \dot{m}_{axial} + \dot{m}_{cool} + \dot{m}_{seeding}$, $\rho(T_{co-flow-ctrl})$ denotes the density of the air at the given co-flow control temperature $T_{co-flow-ctrl}$ (measured at "B" in Fig. 2) at atmospheric pressure and

$D_{O,co-flow}$ and $D_{I,co-flow}$ are the outer and inner diameter of the co-flow, respectively. Bulk velocities for the fuel jet at the burner exit are calculated similarly to the bulk velocities of the co-flow (Eq. (1)).

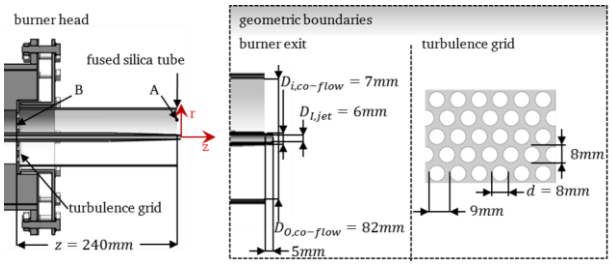

Fig. 2. Cross-section of the burner head exit.

(4) Control unit

The test rig is monitored, actuated and controlled by a CompactRIO real-time control and monitoring device (National Instruments). This control system allows the test rig to be operated in a temperature control mode using $T_{co-flow-ctrl}$ as reference. In this mode the mass flow ratios are kept constant and the microwave power is controlled by a PID-controller to fix the temperature to a user-defined value. The temporal standard deviation of $T_{co-flow-ctrl}$ is below ± 2 K for all operational conditions tested.

Limits of operational range

The application of the MWPH allows a wide range of operational conditions. Classified by $T_{co-flow-ctrl}$ and $u_{co-flow}$, the operational conditions are shown in Fig. 3 along with operational points (markers) for lift-off height (LOH) measurements, which is discussed later. The test rig can be operated at any point of the area defined by limits from A to F in Fig 3.

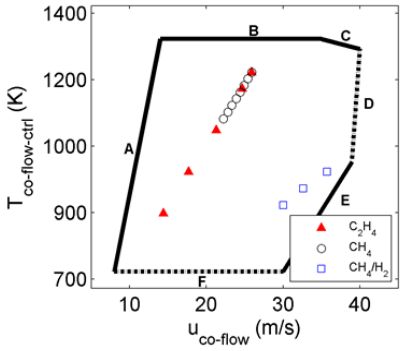

Fig. 3. Operational field of the AI test rig in terms of co-flow velocity and co-flow control temperature.

Limit A marks the slowest operating co-flow velocity possible. It is determined by the minimum air mass flow required for sufficient cooling of the electromagnetic shielding. The maximum operating temperature (limit B) is restricted by the maximum allowed operating temperature of the ceramic insulation of the FCU (1470 K). At high $T_{co-flow-ctrl}$ and high $u_{co-flow}$ the operational conditions are limited by the maximum power output of the magnetron (limit C). Limit D is not reached at high $u_{co-flow}$ and high power output of the MWPH that causes a large plasma volume resulting in potential damage the electromagnetic shielding. Limit E is caused by the maximum $\dot{m}_{co-flow}$. This limit can be extended by exchanging the MFCs. The lower temperature limit F is entailed by strongly increasing reflected microwave power levels in a region of about 725 K, where the power output of the magnetron is relatively low and the plasma has a small fluctuating volume which results in an increasing amount of reflected energy.

Boundary conditions at nozzle exit

Radial cross-sections of the temperature at the burner head exit were characterized with a thermocouple array consisting of five type K thermocouples (2 mm dia.) displaced to each other by 10 mm. Temperatures were sampled every 1 s. Radiation correction based on the energy equation [13] was applied for these measurements. The temperature field was measured on a perpendicular grid with 5 mm spacing centered on the axial centerline with the fuel lance removed. Temperature profiles were measured at two operational points with co-flow control temperatures fixed at 923 K and 1273 K at a co-flow bulk velocity of 30 ms^{-1}. Temperatures were normalized to $T_{co-flow-ctrl}$which is the temperature on the axial centerline at the exit of the fused silica tube ($z = -5$ mm, $r = 0$ mm, see coordinates in Fig. 2). Non-dimensional temperature profiles of $T_{co-flow}/T_{co-flow-ref}$ at two axial positions ($z = -5$ and $z = 55$ mm) are shown in Fig. 4.

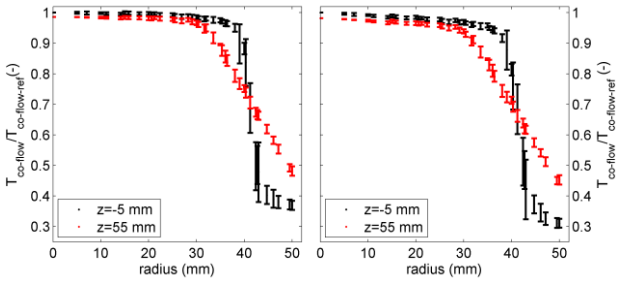

Fig. 4. Normalized radial temperature profiles at two axial positions for (a) $T_{co-flow-ctrl} = 923$ K and b) $T_{co-flow-ctrl} = 1273$ K.

The temperature profiles at $z = -5\ mm$ are close to a top hat with $T_{co-flow} > 0.9 * T_{co-flow-ref}$ for $r < 35$ mm. For radii larger than 35 mm the effect of thermal boundary layers inside the fused silica tube become visible, causing a steep decrease of the temperature within less than 10 mm. Further downstream at $z = 55$ mm, turbulent mixing with cold ambient air reduces the radial extension of the homogenous temperature region to $r < 30$ mm. The co-flow stream is spreading and the temperature decreases within the shear layer that extends over significantly more than 20 mm in radial direction. Measurements of the run-to-run repeatability of the co-flow temperature and further measurements at extended axial positions revealed that up to $z = 115$ mm and $r =$

± 15-20 mm, high reproducibility (deviations below 6%) and spatial homogeneity of the temperature are achieved. This region is sufficiently wide to allow for auto-ignition studies under well-controlled thermal conditions.

Significant amounts of NO and NO_2 are produced by air plasmas at atmospheric pressure [14]. NO_x can influence AI processes of hydrocarbon/air and hydrogen/air mixtures significantly [15-17]. For this reason, NO and NO_2 mole fractions within the co-flow stream were measured at the exit of the burner head using an extractive gas analyzer (Horiba MEXA 1170NX). For each operational point data have been sampled over a duration of 300 s with a sampling rate of approximately 1 s. Fig. 5 shows mean values and standard deviation of NO and NO_2 mole fractions for a variety of operational conditions. Two trends can be noticed. NO and NO_2 mole fractions increased with the increase of temperature. Increasing temperatures are caused by increasing the MWPH power which results in an increased plasma volume that is believed to promote NO and NO_2 production. On the other hand, an increase of NO and NO_2 mole fractions was observed when decreasing the co-flow velocity. This leads to the assumption that NO_x production is influenced by the residence time of the molecules inside the plasma, respectively the recombination zone located at the edge of the plasma torch [18].

The normalized standard deviations of the measurements (represented by error bars in Fig. 5) were in any case below 1.2 %. Furthermore, an evaluation of the run-to-run stability for each operational point showed a repeatability better than ±2 % of the mean NO_x mole fraction. NO mole fractions ranging about 5000 to 10000 ppm, as in the present study, can rise ignition temperatures of hydrogen/air mixtures by approximately 40 K and by 15 K in the case of lean CH_4/air combustion [17]. Therefore, low temperature NO_x chemistry must be included within the reaction mechanisms, when comparing experimental results from the present test rig with numerical simulations.

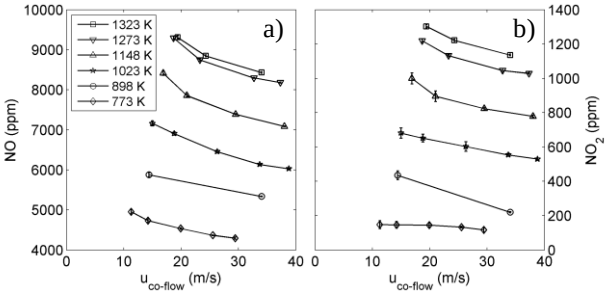

Fig. 5. Mole fraction of (a) NO and (b) NO_2 in the air co-flow at the exit of the burner head ($z = -5$ mm) at different operational conditions.

Lift-off height (LOH) Measurements

During AI processes isolated flame kernels emerge upstream of the lifted flame. The distance from the nozzle at which these kernels appear can be defined as lift-off-height (LOH). The dynamic chemistry-turbulence interactions contribute to fluctuations observed for LOH experiments. A more detailed understanding is currently intended through ongoing laser diagnostic measurements of the local flow properties, markers for low- and high-temperature chemistry such as formaldehyde and OH, and temperature field.

Re and temperature of the co-flow as well as the Re and composition of the fuel jet were varied to perform parametric investigation of the LOH. The specific operating conditions (named by capital letters) are listed in Table 1. Operational conditions from A to J and from T to Y are plotted in Fig. 3. CH_4, C_2H_4, and CH_4/H_2 (50/50 vol-%) mixture were used as fuel for the inner jet. The Re-numbers of the co-flow $Re_{co-flow}$ were 10000 for CH_4 and C_2H_4 and 20000 for CH_4/H_2. Re-numbers of co-flow and fuel are based on the bulk velocities, kinematic viscosities at $T_{co-flow-ctrl}$ and T_{jet}, and on hydraulic diameters of the annular slot and fuel lance at nozzle exit, respectively.

Table 1. Operating conditions (capital letters) with corresponding mean jet temperature (T_{jet}(K)) in brackets.

	Re_{jet} (-)						
$T_{co-flow-ctrl}$ (K)	2000	3000	4000	5000	6000	10000	20000
898	-	-	-	-	-	T(482.0±1.0)[3]	-
923	-	K(524.0±2.8)[1]	-	N(485.5±1.3)[1]	Q(472.5±0.5)[1]	-	-
973	-	L(575.8±1.5)[1]	-	O(513.0±0.8)[1]	R(491.0±0.8)[1]	-	-
1023	-	M(600.0±4.5)[1]	-	P(530.0±0.8)[1]	S(504.8±0.5)[1]	U(525.3±1.2)[3]	-
1148	-	-	-	-	-	V(573.7±1.5)[3]	-
1183	A(792.7±2.5)[2]	-	-	-	-	-	-
1203	B(792.0±2.0)[2]	-	-	-	-	-	-
1223	C(801.7±5.5)[2]	-	-	-	-	-	-
1243	D(814.7±1.1)[2]	-	-	-	-	-	-
1263	E(838.7±3.2)[2]	-	-	-	-	-	-
1273	-	-	-	-	-	W(618.7±0.6)[3]	-
1283	F(860.0±4.6)[2]	-	-	-	-	-	-
1303	G(879.5±3.5)[2]	-	-	-	-	-	-
1323	H(892.0±1.0)[2]	-	I(755±0.0)[2]	-	J(683.3±0.6)[2]	X(527.7±0.6)[3]	Y(527.7±2.3)[3]

[1] Fuel: CH_4/H_2 (50/50 Vol-%), $Re_{co-flow}$=20000, optical setup (a). [2] Fuel: CH_4, $Re_{co-flow}$=10000, optical setup (b).

[3] Fuel: C_2H_4, $Re_{co-flow}$=10000, optical setup (b).

Chemiluminescence (CL) imaging has been proven as a method for LOH measurements [19]. CL was recorded by a high speed camera (LaVision GmbH, HSS5). Two different optical setups were used for different magnification. First (a) a Carl Zeiss Planar T* lens (f=85, f/1.4) with a 12 mm auto extension ring was used at a working distance of 575 mm. For the second setup (b) a Nikkor lens (f=50 mm, f/1.2) with an 8 mm extension ring and a working distance of 385 mm was used. The chip resolution was 1024 x 528 px², which resulted in fields of view (FOV) of 110 x 56 mm² in case (a) and 128 x 66 mm² in case (b). High speed (HS) measurements at 6 kHz where used to study the temporal evolution of propagating AI kernels. The low speed (LS) recordings at 50 Hz were employed to catch statistically independent AI events. Exposure time was fixed at 1/6000 s for all cases. Each dataset consists of 3971 images. Background subtraction was performed for single-shot images using the mean of 500 images without fuel injection (no flame present). To track the AI kernels, an individual adaptive intensity threshold, $I_{thresh,i}$, was computed for each individual CL image as:

$$I_{thresh,i} = I_{base,i} + p_{thresh} * \left(I_{flame,i} - I_{base,i}\right) \quad (2)$$

Where $I_{base,i}$ is the base intensity of the no-flame region (see rectangles marked with "base" in Fig. 6). $I_{flame,i}$ is the maximum occurring intensity inside the "flame" area in Fig. 6 and p_{thresh} is the threshold level, set to 5 % in this case. I_{thresh} is computed by averaging $I_{thresh,i}$ over the whole number of images of each dataset. The binarization of the individual image using I_{thresh} allowed extracting the flame front of the AI kernels and measuring the LOH (Fig. 6).

Fig. 7 presents the results of the structure and temporal evolution of the lifted flame for operational point C. Individual gas pockets appear in the recorded images as flame kernels downstream of the fuel lance exit. These isolated flame kernels propagate downstream, expand, and merge finally to form the base of a lifted flame. Such a visual inspection based on high speed imaging shows that flame stabilization for this operational condition is supported substantially by auto-ignition rather than pure flame propagation [2].

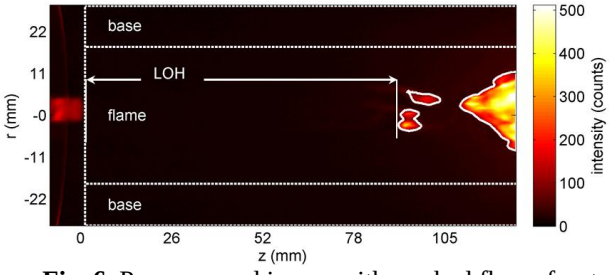

Fig. 6. Preprocessed image with marked flame front (white solid line) and detected LOH. Flow direction is from left to right.

An evaluation at high speed (6 kHz) of the variation of the LOH as a function of time revealed that, depending on the operational conditions, the LOH position fluctuates in a range of approximately 20 to 40% of the mean LOH value. However, results from four individual data sets recorded at high and slow speed, did not show temporal drifts of the median and fluctuations of the LOH. This reflects the stability of the test rig in terms of the co-flow and fuel temperature as well as the NO and NO_2 mole fractions.

In order to investigate the influence of the fuel jet temperature upon the LOH, a separate heating unit was used to vary T_{jet} from 463 to 576 K for operational conditions of point Q. This increase of T_{jet} resulted in a rising of only 14% of the mean LOH. Additionally to discard any thermal decomposition of the fuel, wall temperatures of inner surface of the fuel lance were measured at the nozzle exit using thermographic phosphors [20]. A maximum wall temperature of 987 K was measured for the operational point H (highest T_{jet} =892 K). This value is lower than the calculated temperatures of thermal decomposition of CH_4, C_2H_4 and CH_4/H_2, namely, 1260 K, 1135 K and 1270 K respectively.

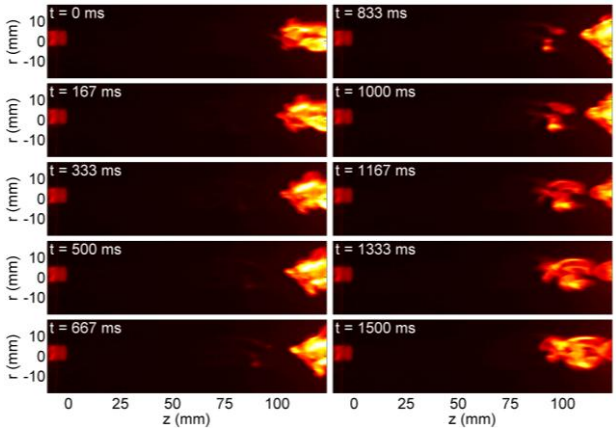

Fig. 7. Consecutive CL images of a CH_4-jet into a hot turbulent air co-flow ($T_{co-flow-ctrl}$ =1223 K) recorded at 6 kHz. Flow direction is from left to right.

The high sensitivity of LOH with respect to $T_{co-flow}$ is demonstrated in Fig. 8 for the mixture CH_4/H_2 (50/50 vol.-%) at different Re of the fuel jet. By increasing the co-flow control temperature $T_{co-flow-ctrl}$ by 100 K from 923 K to 1023 K, the median LOH decreases substantially by 34 mm (Re_{jet}= 3000), 32 mm (Re_{jet}= 5000) and 45 mm (Re_{jet}= 6000). This corresponds to a decline of the median LOH of 68 %, 62 % and 69 % for the Re_{jet} of 3000, 5000 and 6000 respectively. In comparison, the influence of different Re_{jet} upon the LOH is much less pronounced. Rising Re_{jet} from 3000 to 6000 at fixed $T_{co-flow-ctrl}$ increases the median LOH only by 19.2 % ($T_{co-flow-ctrl}$ = 923 K), 14 % ($T_{co-flow-ctrl}$ = 973 K) and 22 % ($T_{co-flow-ctrl}$ =

1023 K). This leads to the conclusion that the AI will most likely take place in regions of the flow field where the co-flow dominates the conditions of the mixture.

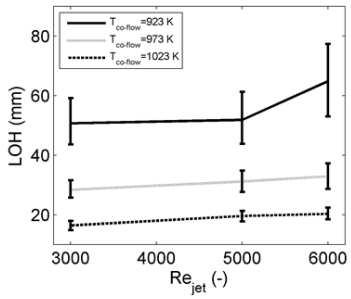

Fig. 8. Median and fluctuations of LOH of CH_4/H_2 mixtures (operational points from K to S) as a function of $T_{co-flow-ctrl}$ and Re_{jet}.

The comparison between the LOH of a CH_4 and a C_2H_4 jets is shown in Fig. 9. The co-flow control temperature was varied between 898 K and 1323 K. $Re_{co-flow}$ was fixed to 10000 for both cases. Re_{jet} was 2000 and 10000 for CH_4 and C_2H_4, respectively. At the highest achievable co-flow temperatures ($T_{co-flow-ctrl}$= 1323 K), the LOH of the C_2H_4 flame reaches 10 mm whereas it is still at 60 mm for CH_4. The decreases on sensitivity of the LOH when increasing $T_{co-flow}$ is more obvious for the lifted C_2H_4 flame. This is attributed to the Arrhenius-like character of the underlying elementary reactions.

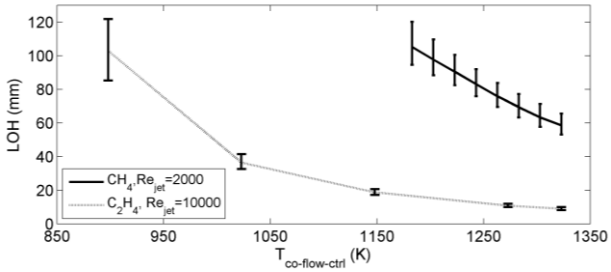

Fig. 9. Median and fluctuations of LOH of CH_4 (operational points from A to H) and C_2H_4 (operational points from T to X) jets as a function of $T_{co-flow-ctrl}$.

Conclusions

The developed test rig based on plasma-heating (MWPH) is well suited for experimental auto-ignition investigations at high turbulence levels along a wide range of co-flow temperatures and velocities using a variety of fuels, even CH_4. The system is characterized by a high repeatability of the thermal inflow conditions of the co-flow. As a side effect, relatively high mole fraction levels of NO and NO_2 are produced that must be considered for interpretation of the results and comparison to numerical simulations. First experimental studies of the lift-off height (LOH) of a CH_4, C_2H_4 and CH_4/H_2 showed that the flame stabilization mechanism in this specific configuration is supported substantially by auto-ignition rather than pure flame propagation. Increasing co-flow temperature the LOH decreases substantially. The fluctuation level of LOH decreases with decreasing mean LOH-values for all investigated operational points. Increasing the fuel jet Re-number results in a slight increase of LOH. This means that the conditions of the co-flowing air dominate the AI process in the current experimental setup.

Acknowledgements

We gratefully acknowledge financial support by DFG (DR 374/8-1) and the Excellence Initiative, Darmstadt Graduate School of Excellence Energy Science and Engineering (GSC 1070). Fruitful discussions with E. Mastorakos, C. Markides and Martina Leins are appreciated. We are thankful for an intense cooperation with Mügge GmbH, Germany, during design of the MWPH.

References

[1] N. Milovanovic, R. Chen, SAE Paper 2001-01-1890 (2001).

[2] E. Mastorakos, Prog. Energy Combust. Sci. 35 (2009) 57-97.

[3] E. Mastorakos, T.A. Baritaud, T.J. Poinsot, Combust. Flame 109 (1997) 198-223.

[4] R. Kulkarni, W. Polifke, J. Combust. 2012 (2012) 1-11.

[5] C.N. Markides, E. Mastorakos, Proc. Combust. Inst. 30 (2005) 883-891.

[6] R.L. Gordon, A.R. Masri, E. Mastorakos, Combust. Flame 155 (2008) 181-195.

[7] E. Oldenhof, M.J. Tummers, E.H. van Veen, D.J.E.M. Roekaerts, Combust. Flame 157 (2010) 1167-1178.

[8] B.C. Choi, S.H. Chung, Combust. Flame 159 (2012) 1481-1488.

[9] C.N. Markides, G. De Paola, E. Mastorakos, Exp. Therm. Fluid Sci. 31 (2007) 393-401.

[10] R.L. Gordon, A. Masri, E. Mastorakos, Combust. Theory Model. 13 (2009) 645-670.

[11] C. Tendero, C. Tixier, P. Tristant, J. Desmaison, P. Leprince, Spectrochim. Acta Part B At. Spectrosc. 61 (2006) 2-30.

[12] Q. Jin, C.H.U. Zhu, M.W. Borer, G.M. Hieftje, Spectrochim. Acta 46B (1991) 417-430.

[13] M.J. Dunn, A.R. Masri, R.W. Bilger, Combust. Flame 151 (2007) 46-60.

[14] C.M. Du, J.H. Yan, B. Cheron, Plasma Sources Sci. Technol. 16 (2007) 791-797.

[15] F.N. Egolfopoulos, P.E. Dimotakis, Combust. Sci. Technol. 156 (2000) 173-199.

[16] K. Takita, N. Abe, G. Masuya, Y. Ju, Proc. Combust. Inst. 31 (2007) 2489-2496.

[17] Y. Tan, C.G. Fotache, C.K. Law, Combust. Flame 119 (1999) 346-355.

[18] M. Leins, Private Communication (26.09.2013).

[19] K.N. Kim, S.H. Won, S.H. Chung, Proc. Combust. Inst. 31 (2007) 947-954.

[20] J. Brübach, C. Pflitsch, A. Dreizler, B. Atakan, Prog. Energy Combust. Sci. 39 (2013) 37-60.